ISTITUTO NAZIONALE DI FISICA NUCLEARE

LABORATORI NAZIONALI DI FRASCATI

INFN-14-05/LNF
25th March 2014

DEFLECTION OF PROTON BEAMS BY CRYSTAL MISCUT SURFACE

A.A. Babaev[1,2], and S.B. Dabagov[3,4]

[1]*INFN Sezione di Roma, Rome, Italy*
[2]*Tomsk Polytechnic University, Tomsk, Russia*
[3]*INFN Laboratori Nazionali di Frascati, Frascati, Italy*
[4]*RAS P.N. Lebedev Physical Institute & NRNU MEPhI, Moscow, Russia*

Abstract

The theory of beam deflection by the terrace crystal field forming the miscut surface was developed. The phenomenology of proton channeling and quasichanneling has been applied to describe new features of the beam deflection. The computer experiment results on proton beam deflection by the crystal miscut surface are presented. The analysis predicts efficient beam deflection by the acute crystal end due to repelling miscut potential.

Published by ***SIDS–Pubblicazioni***
Laboratori Nazionali di Frascati

Submitted to *Physical Review ST Accelerators and Beams*

1. INTRODUCTON

1.1. Channeling-related effects in accelerator physics

One of the most important problems in accelerator physics is known as a beam collimation problem, which includes the beam shaping, the halo removing, etc. Usually to improve the beam quality the complex system of magnets as well as solid collimators and beam scrapers are used. The methods based on bent crystal technology open new ways to efficient control the proton or heavy ion beams especially at ultra-high energies [1,2]. The applicability of bent crystal collimators is based on the effective particle deflection in the crystal volume due to the planar channeling [3,4] or volume reflection [5,6] phenomena. In general, both effects take place when fast charged particles penetrate into the crystal at small glancing angle θ_0 to crystallographic planes. In this case the motion of a fast projectile is characterized as a quasi free longitudinal motion inside the crystal being transversally trapped by so-called averaged planar potential [7,8].

For positively charged particles the averaged potential of a single plane has the maximum at the plane position, decreases rapidly at the increase of the distance from it, and, finally, the electric field becomes negligible at the inter planar distance. Thus, two neighboring planes form the potential well with the minimum between them.

The particle channeling takes place if $E_{\mathrm{tr}}(\theta, x_{\mathrm{ch},0}) < U_{\mathrm{ch},0}$, where $E_{\mathrm{tr}}(\theta_0, x_{\mathrm{ch},0})$ is the particle transverse energy (see [8] and Sec.2.1.1 below). It depends on the initial particle position in the channel $x_{\mathrm{ch},0}$ and glancing angle θ_0. The planar channeled particle is trapped by the potential well between two adjacent planes and moves along these planes oscillating between them. The channeling is impossible if $\theta_0 > \theta_L$, where at the particle ultra-relativistic energies E the critical angle $\theta_L = \left(2U_{\mathrm{ch},0} / E\right)^{1/2}$, known as Lindhard angle. Nevertheless, if $\theta_0 < \theta_L$ and simultaneously $E_{\mathrm{tr}}(x_0, \theta_0) > U_{\mathrm{ch},0}$ the particle trajectory is not bound within a single planar channel although, the motion is still governed by the averaged potential. This regime of motion is called quasichanneling. The quasichanneling conception is valid also at $\theta_0 > \theta_L$ if the incident angle θ_0 is of the order of a few critical angles θ_L. The volume reflection appears for a quasichanneled particle at specific conditions [9,10].

The demands of fine-tuned beam management require very accurate manipulations for a crystal positioning into the beam. In particular, the crystal has to be inserted into the beam at very small distance providing very small impact parameters (i.e. the distances from the crystal edge along the crystal entrance face to the point where the particles hit the crystal). For example, in experiment [3] the averaged impact parameter was estimated to be of the order of 100 nm. Hence, the particles hitting the lateral crystal surface instead of expected front surface can essentially influence the crystal merits to deflect the beam. The lateral surface considered here is directed along the beam propagation making small grazing angle. Thus, moving the crystal into the beam the particles first interact with the lateral surface that makes important studying the features of beam interaction with the crystal surface at small glancing angles.

2.2. Crystal miscut surface

In principle, the crystals available for modern experiments have almost perfect flat surfaces [11,12] characterized by the ordered atoms location. The angular asymmetry of beam scattering by crystal surface as well as the periodicity in the energy loss spectra of scattered beam were discovered almost together with the channeling effect and witness to the ordered surface lattice [13–15]. The surface channeling was discussed in [15] when the particle can be first captured into the channeling motion at a surface layer and successfully leaves the crystal through the same lateral surface. Moreover, as shown in [16–19] the averaged field approximation is valid for

description of particle small angle scattering by a crystal surface, which coincides with one of the main crystallographic planes. Recent experiments on surface both scattering and channeling were mostly carried out for nonrelativistic light ions. The beam interaction with crystal atomic chains (axial effects) [20–25] as well as planes (planar effects) [19,24–26] has been carefully analyzed within various collaborations.

This work is devoted to studying ultra relativistic particles scattering by lateral crystal surface. The scheme of scattering has been suggested by the geometry of beam collimation experiments. The beam is oriented at small angle (or parallel) to crystallographic planes to satisfy the planar channeling conditions but at large enough angles to the main crystallographic axes to avoid the axial channeling (see, for example, in [27, 28]).

Crystals used in crystal collimation experiments are usually characterized by the lateral surface not parallel to crystallographic planes responsible for the particle channeling in a crystal bulk. The angle between the lateral surface and mentioned planes is known as a miscut angle [9,29,30], while the surface has been called a miscut surface (Fig. 1(a)). This surface is structured by a set of parallel planes that form stepped terraces; each terrace of the length Δz is a part of the crystal plane, while a step equals to the inter planar distance a (Fig. 1(b)). Obviously, the miscut angle θ_m defined by such geometry is extremely small. Positively charged beam hitting the miscut surface of aligned crystal will undergo multiple terrace reflection.

Let consider fast particles of non-divergent beam hitting the crystal surface along the crystallographic planes, as shown in Fig. 1. If the entry surface has no miscut (the planes are perpendicular to the surface), the particles entering the crystal at channeling conditions become trapped between the planes that define the potential well. On the contrary, in the case of nonzero miscut angle the particles hitting the miscut surface first interact with averaged potential of a single plane that defines the terrace. In our case, protons are reflected by the repelling plane field (terrace potential) outward of the plane. Obviously, we can define three different regimes of proton motion. The first one corresponds to the case when a proton is strongly deflected providing its interaction with next plane (surface potential of upper terrace) instead of averaged channel potential (bulk potential) of adjacent planes, which form lower (actual) and upper terraces (Fig. 1(b), arrow 1). Both second and third regimes take place when the deflection of a proton is not enough to be out of corresponding planar channel. If herein the transverse energy counted from the center of channel is less than $E\theta_L^2/2$ (see below in Sec. 2.3.2) the proton will move in a crystal volume being planar channeled (Fig. 1(b), arrow 2). Otherwise the proton becomes quasichanneled and will suffer a kind of volume reflection (Fig. 1(b), arrow 3). The kind of motion depends on the initial particle distance to the nearest lower plane at the moment when the particle starts interacting with the crystal field. In general case, all described regimes exist when the beam hits the miscut surface.

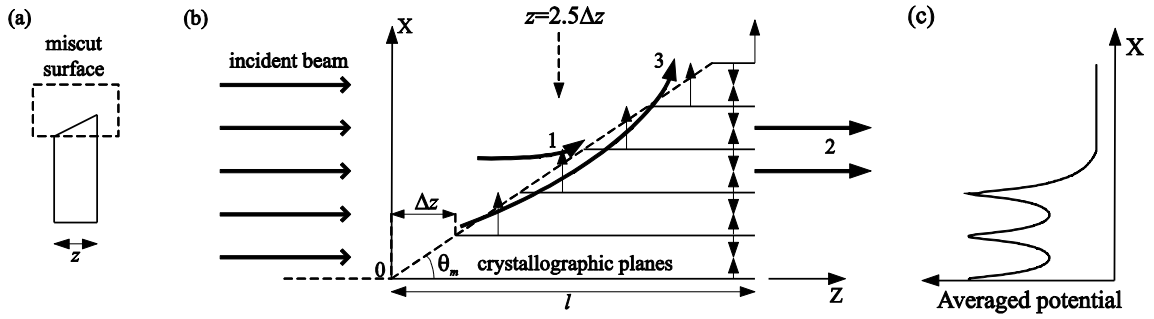

Fig.1. (a) Scheme of the crystal with a miscut surface. The crystal has the trapezium shape; the miscut surface is the top triangle part of the trapezium. (b) Scheme of beam deflection by the miscut surface. The crystal field affecting the particle is either the deflecting field at the beginning section Δz or is the planar channel field (the direction of the field is pointed out by thin vertical arrows). The regimes of a particle motion are pointed out by the bold arrows: 1 — the particle deflected outward the miscut surface by the repelling potential of the terraces; 2 —

the channeled particles penetrating into the surface layer and successfully leaving the crystal through the back end; 3 — the particles deflected via quasichanneling. (c) Scheme of averaged potential $U_{cr}(x)$ at the longitudinal coordinate z = 2.5 Δz pointed out by dash arrow in the panel (b).

In the Part 2 of the preprint the motion of ultra-relativistic proton in the field of single terrace will be considered for the case when the terrace potential is approximated by the harmonic potential. The conditions of channeling and quasichanneling are analyzed. In the Part 3 the results of numerical simulations for the case of Moliere potential is presented. The role of multiple terrace deflection is discussed.

2. GENERAL THEORY BASED ON MODEL HARMONIC POTENTIAL

This part is devoted to the theoretical consideration of particle motion in the field of single terrace. The crystal potential is approximated by model harmonic potential to obtain the analytical solutions of motion equation. The analytical solution gives the possibility to make the general conclusions as well as estimations on the particle motion.

2.1. General points

Let consider below the motion of ultra-relativistic protons in the field of acute channel, i.e. in the field of single terrace. The terrace length Δz is large enough to consider the field as orthogonal to the plane as well as to describe the field by the averaged potential. The terrace field depends on transverse coordinate x only. The coordinate frame is designated in Fig. 1(b). The proton initially penetrates into the field along planes.

Concerning the terrace field, it is suggested the field becomes negligible at the distance a from the plane. The terrace potential barrier with respect to the vacuum is $U_{pl,0}$, the channel potential deep is $U_{ch,0}$; $U_{pl,0} = U_{ch,0} + \Delta U$, where ΔU is the crystal potential in the channel center.

2.1.1. Energy conservation

The energy of a free particle can be written as

$$\gamma mc^2 = \sqrt{m^2c^4 + p_z^2c^2 + p_x^2c^2} = \sqrt{m^2c^4 + p_z^2c^2\left(1+\theta^2\right)},$$

where p_z p_x are momentum projections onto corresponding axes, m is the rest mass. For the case of ultrarelativistic particle considered here $p_x = p_z$, $p_x = p_z\theta$, θ is the small angle between longitudinal and transverse momentum. It can be interpreted as the deflection angle. Hence, approximately,

$$\gamma mc^2 \approx \sqrt{m^2c^4 + p_z^2c^2}\left(1+\frac{p_z^2c^2\theta^2}{2\left(m^2c^4 + p_z^2c^2\right)}\right).$$

In the ultra-relativistic case $p_zc >> mc^2$ and, therefore,

$$\gamma mc^2 = p_zc\left(1+\frac{\theta^2}{2}\right).$$

The full energy of particle is conserved:

$$E = \gamma mc^2 + U_{cr}(x).$$

At the initial point of trajectory $\theta = 0$ and $x = x_0$. For the arbitrary moment of the motion in terrace field the energy conservation low gives

$$\frac{p_z c\theta^2}{2} + U_{\text{cr}}(x) = U_{\text{cr}}(x_0). \tag{1}$$

Hence, the deflection angle can be defined from the expression:

$$\theta = \sqrt{\frac{2\left(U_{\text{cr}}(x_0) - U_{\text{cr}}(x)\right)}{p_z c}}. \tag{2}$$

The left hand side of Eq.(1) is namely the transverse energy:

$$E_{\text{tr}}(\theta, x) = \frac{p_z c\theta^2}{2} + U_{\text{ch}}(x)$$

2.1.2. Transverse motion

The transverse momentum of projectile should be evaluated from the motion equation

$$\frac{dp_x}{dt} = -\frac{dU_{\text{cr}}(x)}{dx}.$$

The longitudinal proton velocity $v_z \approx c$. Hence, the motion equation can be rewritten as

$$p_z c \frac{d\theta}{dz} = -\frac{dU_{\text{cr}}}{dx}, \tag{3}$$

where the relation $dt = dz / v_z \approx dz / c$ was used. The longitudinal momentum is considered constant.

2.1.3. Trajectory

From the Eq. (2) one can obtain

$$\frac{d\theta}{dz} = -\frac{1}{\sqrt{2 p_z c\left(U_{\text{cr}}(x_0) - U_{\text{cr}}(x)\right)}} \frac{dU_{\text{cr}}}{dx} \frac{dx}{dz}.$$

The substitution of this relation into Eq. (3) gives the trajectory equation:

$$\frac{dx}{\sqrt{U_{\text{cr}}(x_0) - U_{\text{cr}}(x)}} = \sqrt{\frac{2}{p_z c}} dz.$$

Hence, the transverse coordinate x in the moment when the projectile has the longitudinal coordinate is z should be defined from the equation

$$\sqrt{\frac{2}{p_z c}} z = \int_{x_0}^{x} \frac{dx}{\sqrt{U_{\text{cr}}(x_0) - U_{\text{cr}}(x)}}. \tag{4}$$

2.2. Harmonic potential and projectile trajectory

The harmonic terrace potential in the range $0 \le x \le a$ is described by the function

$$U_{\text{pl}}(x) = U_{\text{pl},0}\left(1 - \frac{x^2}{a^2}\right),$$

it equals to 0 at $x = a$ (at $x > a$ the crystal field becomes zero) and it equals to $U_{\text{pl},0}$ at $x = 0$ (at $x < 0$ the crystal field is exactly the channel field), see in Fig. 2.

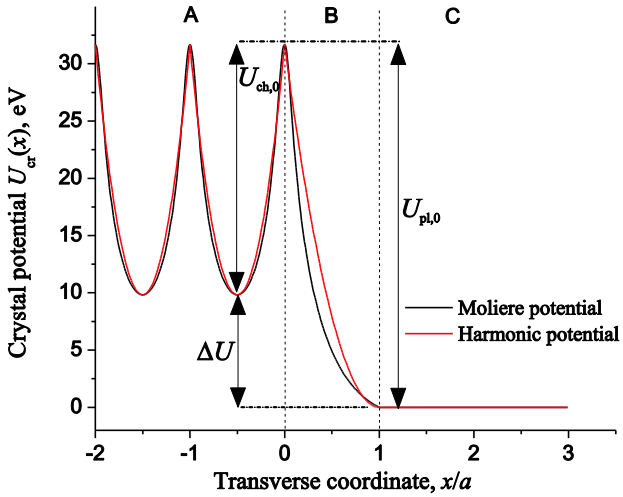

Fig.2. Averaged potential $U_{\rm cr}(x)$ near the lateral crystal surface formed by (110) Si planes: A - channel potential; B - terrace potential; C - $U_{\rm cr}=0$. The surface potential barrier is $U_{\rm pl,0}=31.7$ eV, the inter planar channel deep is $U_{\rm ch,0}=21.9$ eV and the potential at the channel center with respect to zero level is $\Delta U=9.8$ eV.

If the particle penetrate into the crystal field having the transverse coordinate x_0, its transverse coordinate $x \geq x_0$ while the particle moves through the terrace field. Hence,

$$\int_{x_0}^{x} \frac{dx}{\sqrt{U_{\rm cr}(x_0)-U_{\rm cr}(x)}} = \frac{a}{\sqrt{U_{\rm pl,0}}}\left(\frac{\pi}{2}-\arcsin\frac{1-y}{1-y_0}\right),$$

where $y=x/a$ and $y_0=x_0/a$. Eq.(3) therefore gives

$$\frac{\pi}{2}-\arcsin\frac{1-y}{1-y_0}=\sqrt{\frac{2U_{\rm pl,0}}{p_z c}}\,\frac{z}{a}.$$

Obviously, one can introduce the characteristic angle

$$\theta_{\rm pl}=\sqrt{\frac{2U_{\rm pl,0}}{p_z c}}$$

in analogy with the Lindhard angle θ_L. The angle $\theta_{\rm pl}$ is the critical glancing angle for the particle penetrating into the crystal volume through the lateral surface. I.e. the particle can cross the lateral potential barrier if it has the glancing angle $\theta>\theta_{\rm pl}$. Otherwise it will be reflected outward the surface.

The particle trajectory in the terrace field is the branch of sine wave:

$$y=1-(1-y_0)\cos\left(\theta_{\rm pl}\frac{z}{a}\right). \qquad (5)$$

This solution is valid for $0\leq y_0\leq 1$, the transverse coordinate $y_0\leq y\leq 1$, the longitudinal coordinate $0\leq z\leq \Delta z$ where $\Delta z=a/\tan\theta_m$ is the length of plane section responsible for the repelling field, above named as a terrace, see in Fig.1.

2.3. Projectiles motion

2.3.1. The deflection by terrace potential

The feature of solution (5) is all trajectories cross at the same point if Δz is large enough, see in Fig.3. The crossing point is defined as one-fourth from the oscillation period in Eq. (5), i.e. the intersection point is at the distance

$$z_{\text{is}} = \frac{\pi a}{2\theta_{\text{pl}}} \tag{6}$$

from the point where particles penetrate into the field. If $z_{\text{is}} < \Delta z$ all particles can not reach the channel, they are deflected outward the lateral surface. This case was designated as the type 1 in the Sec. 1.2. The exception is only the particle penetrating into the field having $y_0 = 1$. This particle is not influenced by the field and is not deflected.

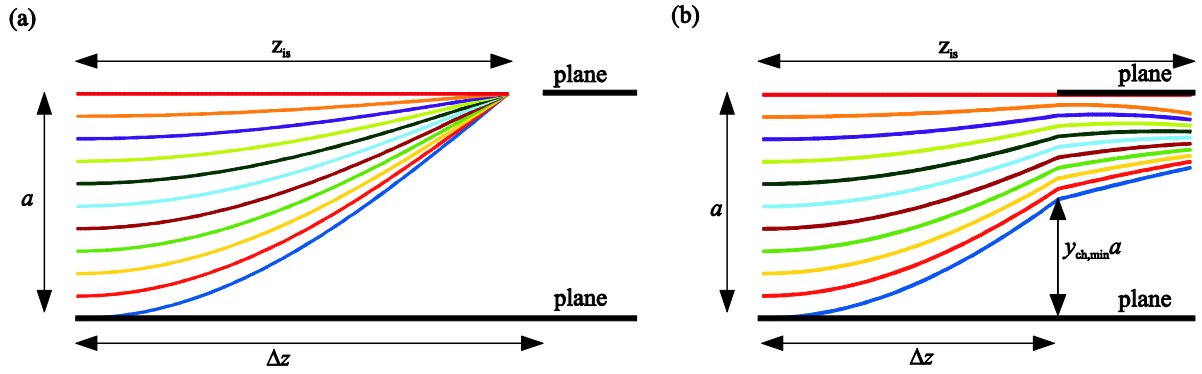

Fig.3. Scheme of particle trajectories in harmonic terrace potential at $0 \le x \le a$: (a) $z_{\text{is}} < \Delta z$, particles can not reach the channel; (b) $z_{\text{is}} > \Delta z$, particles penetrate into the channel field.

The condition (6) allows estimating the critical miscut angle when all particles can not reach the channel (in the assumption this angle remains small):

$$\theta_{m,\text{cr}} = \frac{a}{z_{\text{is}}} = \frac{2\theta_{\text{pl}}}{\pi}. \tag{7}$$

In this case the deflection angles can be defined from Eq. (2)

$$\theta = \theta_{\text{pl}}\left(1 - y_0\right),$$

where the final transverse coordinate is the same for all particles: $y = 1$. Therefore, the deflection angles are $0 \le \theta \le \theta_{\text{pl}}$.

At the miscut angle $\theta_m > \theta_{m,\text{cr}}$ (or, equivalently, $z_{\text{is}} > \Delta z$) all particles reach the channel. Therefore channeling and quasichanneling effects appear. The glancing angle at the channel beginning is defined by the Eq. (2):

$$\theta = \theta_{\text{pl}}\sqrt{\left(1-y_0\right)^2 - \left(1-y\right)^2} = \theta_{\text{pl}}\left(1-y_0\right)\sin\left(\theta_{\text{pl}}\frac{\Delta z}{a}\right) = \theta_{\text{pl}}\left(1-y_0\right)\sin\left(\frac{\theta_{\text{pl}}}{\theta_m}\right) \tag{8}$$

where the trajectory equation (5) was used, $z = \Delta z$ and miscut angle $\tan\theta_m = a/\Delta z$ is small. The minimal incident angle is zero and it corresponds to the no-bent trajectory with $y_0 = 1$. The maximal angle θ belongs to the trajectory with $y_0 = 0$, i.e to the particle penetrating into the terrace field close to the plane:

$$\theta_{\max} = \theta_{\text{pl}}\sin\left(\frac{\theta_{\text{pl}}}{\theta_m}\right).$$

From the other side, from (5) one can evaluate the minimal particle transverse coordinate at the channel entrance (see in Fig. 3b)

$$y_{\mathrm{ch,min}} = 1 - \cos\left(\frac{\theta_{\mathrm{pl}}}{\theta_m}\right). \qquad (9)$$

2.3.2. Channeling and quasichanneling

The type of particle motion in a channel potential – channeling or quasichanneling (type 2 or type 3 correspondingly) - is defined by its transverse energy at the channel entrance. The transverse energy is defined by the left hand side of (1):

$$E_{\mathrm{ch}}(\theta, x) = \frac{p_z c\theta^2}{2} + U_{\mathrm{ch}}(x). \qquad (10)$$

Here $U_{\mathrm{ch}}(x)$ is the channel potential between planes at the point where the particle enters into channel. If the non-equality

$$E_{\mathrm{ch}}(\theta, x) < \frac{p_z c\theta_L^2}{2} + \Delta U \qquad (11)$$

is valid, the particle will be channeled; otherwise it will be quasichanneled. In the last expression ΔU is the value of channel potential at the channel center with respect to zero level of vacuum (see in Fig. 2).

Let consider the harmonic channel potential, i.e.

$$U_{\mathrm{ch}}(x) = U_{\mathrm{ch},0}\left(1 - \frac{2x}{a}\right)^2 + \Delta U = U_{\mathrm{ch},0}\left(1 - 2y\right)^2 + \Delta U. \qquad (12)$$

The form (12) satisfies the conditions $U_{\mathrm{ch}}(0) = U_{\mathrm{ch}}(a) = U_{\mathrm{ch},0} + \Delta U$ and $U_{\mathrm{ch}}(a/2) = \Delta U$.

Using Eqs. (8), (5) and (12) one can write the transverse energy (10) in dependence on the initial particle position $y_{\mathrm{ch},0}$ in the channel:

$$E_{\mathrm{ch}}(y_{\mathrm{ch},0}) = U_{\mathrm{pl},0}\left(1 - y_{\mathrm{ch},0}\right)^2 \tan^2(\theta_{\mathrm{pl}}/\theta_m) + U_{\mathrm{ch},0}\left(1 - 2y_{\mathrm{ch},0}\right)^2 + \Delta U, \qquad (13)$$

$y_{\mathrm{ch,min}} \le y_{\mathrm{ch},0} \le 1$, see in Fig. 4. The same expression in terms of initial coordinate y_0 gives:

$$E_{\mathrm{ch}}(y_0) = U_{\mathrm{pl},0}\left(1 - y_0\right)^2 \sin^2\frac{\theta_{\mathrm{pl}}}{\theta_m} + U_{\mathrm{ch},0}\left(2\left(1 - y_0\right)\cos\frac{\theta_{\mathrm{pl}}}{\theta_m} - 1\right)^2 + \Delta U.$$

Let consider the equality in (11) with the transverse energy E_{ch} described by the last expression:

$$\left(2s_0\cos\frac{\theta_{\mathrm{pl}}}{\theta_m} - 1\right)^2 = 1 - \frac{\theta_{\mathrm{pl}}^2}{\theta_L^2}s_0^2\sin^2\frac{\theta_{\mathrm{pl}}}{\theta_m},$$

where $s_0 = 1 - y_0 = \left(1 - y_{\mathrm{ch},0}\right)/\cos(\theta_{\mathrm{pl}}/\theta_m)$, $U_{\mathrm{pl},0}/U_{\mathrm{ch},0} = \theta_{\mathrm{pl}}^2/\theta_L^2$. This last equation has two roots shown in Fig. 4. The first $s_{01} = 0$ corresponds to the particle penetrating into the field close to the plane. The second s_{02} is defined from the relation

$$s_{02} = \frac{\cos(\theta_{\mathrm{pl}}/\theta_m)}{\cos^2(\theta_{\mathrm{pl}}/\theta_m) + \dfrac{\theta_{\mathrm{pl}}^2}{4\theta_L^2}\sin^2(\theta_{\mathrm{pl}}/\theta_m)}. \qquad (14)$$

One should underline, the coefficient $\theta_{\mathrm{pl}}^2/\theta_L^2$ depends only on crystal properties and does not depend on the particle energy.

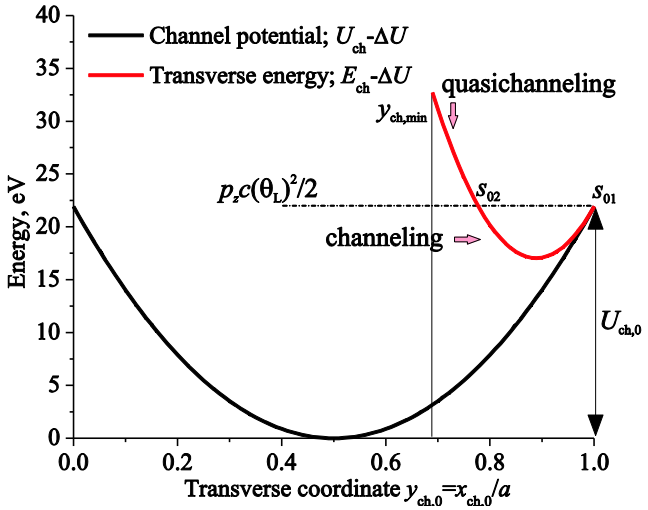

Fig.4. The harmonic (110) Si channel potential (12) shown in Fig. 2 and particle transverse energy (13) at channel entrance. The proton energy is $p_z c = 400$ GeV. Projectiles can have only transverse coordinates $y_{\mathrm{ch,min}} \le y_{\mathrm{ch},0} \le 1$. The horizontal line $p_z c\theta_L^2/2 = U_{\mathrm{ch},0}$ corresponds to equality in relation (11) and crosses the transverse energy curve at points designated s_{01} and s_{02}. Particles having the transverse energy below that line are trapped into channeling motion whereas the transverse energy above means the particle will be quasichanneled. The graph is done for $\theta_m = 10$ μrad. At given conditions following Eq. (9) $y_{\mathrm{ch,min}} = 0.69$.

From Eq.(14) the parameter $s_{02} = 0$ at $\theta_{\mathrm{pl}}/\theta_m = \pi/2$. At this value $y_{\mathrm{ch,min}} = 1$, i.e. particles can not reach the channel. If $s_{02} \neq 0$ the channeling exists for particles with $0 \le s_0 \le s_{02}$ as shown in Fig.4. Hence, while $s_{02} \le 1$ the parameter s_{02} represents the channeled fraction of the incident beam.

From the other hand, when $s_{02} > 1$ (or, equivalently, $y_0 < 0$ and $y_{\mathrm{ch},0} < y_{\mathrm{ch,min}}$) the quasichanneling is not possible, all particles will be trapped in the channeling motion. The equation $s_{02} = 1$ in general case has two roots for $\alpha = \theta_{\mathrm{pl}}/\theta_m$. The first equals to 0. Formally it corresponds to the limit $\theta_m \to \infty$. As the matter of fact, the maximal possible miscut angle is $\theta_{m,\max} = \pi/2$, hence one should take into account the lower limit $\alpha_{\min} = 2\theta_{\mathrm{pl}}/\pi$ for α. The second root $\alpha_{m,\mathrm{qch}}$ defines the specific miscut angle $\theta_{m,\mathrm{qch}}$ so the quasichanneling is impossible for $\theta_m > \theta_{m,\mathrm{qch}}$ (i.e. for $\alpha_{\min} < \alpha < \alpha_{m,\mathrm{qch}}$). Indeed, for large miscut angle the length Δz is very small and projectiles can not obtain the enough transverse energy to be quasichanneled while they move in the terrace potential before the channel entrance. The dependence $s_{02}(\alpha)$ is shown in Fig. 5 for $p_z c = 400$ GeV protons. The curve falls to zero at $\alpha = \pi/2$ when miscut angle equals to $\theta_{m,\mathrm{cr}}$, see Eq. (7).

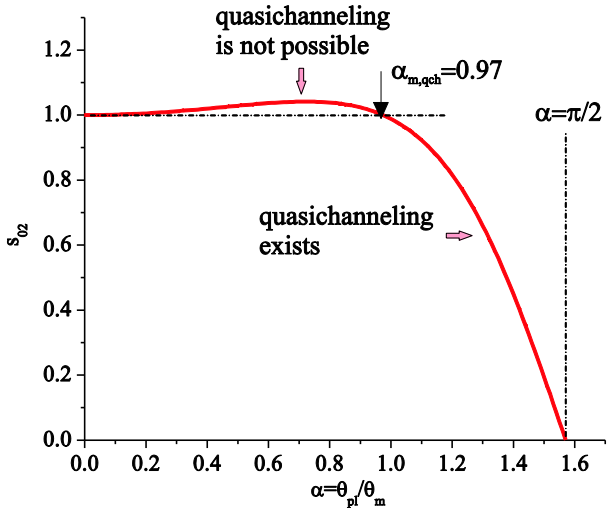

Fig.5. The dependence $s_{02}(\theta_{\rm pl}/\theta_m)$, Eq. (14), for $p_z c = 400$ GeV protons and (110) oriented Si crystal. In the graph $\alpha = \theta_{\rm pl}/\theta_m$, at these conditions $\alpha_{\rm min} = 8\cdot 10^{-6}$. The curve crosses the line $s_{02} = 1$ at $\alpha = 0$ and $\alpha = \alpha_{m,\rm qch} = 0.97$ which corresponds to $\theta_{m,\rm qch} = 13$ μrad. The quasichanneling is not possible for $0 < \alpha < \alpha_{m,\rm qch}$ when $s_{02} > 1$.

More correctly, at large miscut one should consider $\alpha = \theta_{\rm pl}/\tan\theta_m$ instead of $\alpha = \theta_{\rm pl}/\theta_m$ so the lower limit $\alpha_{\rm min} \to \infty$. But in all interesting cases both the miscut angle and $\alpha_{\rm min}$ are small.

From the Eq. (14) on can conclude the shape of curve in Fig.5 at $0 < \alpha < \pi/2$ does not depend on projectile energy. It is defined completely by the ratio $U_{\rm pl,0}/U_{\rm ch,0}$, i.e by crystal properties. The curve has the maximum at α' that could be defined from the equation

$$\tan^2\alpha' = \frac{4U_{\rm ch,0}}{U_{\rm pl,0}} - 2.$$

If for certain crystal $U_{\rm pl,0} = 2U_{\rm ch,0}$, hence $\alpha' = 0$, i.e. the maximum of s_{02} curve coincides with the initial point at $\alpha = 0$, $s_{02}(\alpha) = \cos\alpha$. Hence for this crystal the quasichanneling exists at any ultrarelativistic energy (while the theory described in Sec. 2.1.1. is applicable). In general, the same conclusion is valid for crystals with $U_{\rm pl,0} \geq 2U_{\rm ch,0}$.

To conclude the discussion of the Eq. (14) one should mention that in all possible cases $U_{\rm pl,0} > U_{\rm ch,0}$ and, therefore, $\theta_{\rm pl}^2/(4\theta_L^2) > 0.25$.

2.4. Estimations

Estimations below is done for (110) oriented Si crystal. The potential parameters are: the surface potential barrier is $U_{\rm pl,0} = 31.7$ eV, the interplanar channel deep is $U_{\rm ch,0} = 21.9$ eV, see also Fig.2. The distance between neighboring planes is $a = 1.92$ angstroms.

2.4.1. 400 GeV protons

The critical angles are $\theta_{\rm pl} = 12.6$ μrad, $\theta_L = 10.5$ μrad. The distance of beam focusing by the terrace field is $z_{\rm is} = 23.9$ μm, the corresponding critical miscut is $\theta_{m,\rm cr} = 8$ μrad, i.e. at $\theta_m < 8$ μrad both channeling and quasichanneling are impossible. The maximal deflection angle at $\theta_m < 8$ μrad equals to 12.6 μrad.

From the equation $s_{02} = 1$ one can evaluate another critical miscut angle, namely, $\theta_{m,\mathrm{qch}} = 13$ μrad. At $\theta_m > 13$ μrad all protons are channeled, whereas at $8 < \theta_m < 13$ μrad both channeling and quasichanneling exist, see in Fig.5.

Let consider $\theta_m = 10$ μrad. Eq.(9) gives $y_{\mathrm{ch,min}} = 0.69$ for minimal transverse coordinate of starting point of protons that reach the channel, see in Fig.4. The channeled fraction can be found from Eq.(14): $s_{02} = 0.73$, i.e. quasichanneled fraction is 0.27 of whole beam intencity.

2.4.2. 120 GeV protons

The critical angles are $\theta_{\mathrm{pl}} = 23$ μrad, $\theta_L = 19.1$ μrad. The distance of beam focusing by the terrace field is $z_{\mathrm{is}} = 13.1$ μm, the corresponding critical miscut angle is $\theta_{m,\mathrm{cr}} = 14.6$ μrad, i.e. at $\theta_m < 14.6$ μrad both channeling and quasichanneling are impossible. The maximal deflection angle at $\theta_m < 14.6$ μrad equals to 23 μrad.

The shape of $s_{02}(\theta_{\mathrm{pl}} / \theta_m)$ curve does not depend on the proton energy; it depends only on crystal properties, see Eq.(14). Hence, the critical miscut angle $\theta_{m,\mathrm{qch}}$ can be found using the curve shown in Fig.5: $\theta_{m,\mathrm{qch}} = \theta_{\mathrm{pl}} / 0.97 = 23.7$ μrad. At $\theta_m > 23.7$ μrad all protons are channeled, whereas at $14.6 < \theta_m < 23.7$ μrad both channeling and quasichanneling exist.

Let consider $\theta_m = 20$ μrad. Eq.(9) gives $y_{\mathrm{ch,min}} = 0.62$ for minimal transverse coordinate of starting point of protons that reach the channel. The channeled fraction can be found from Eq.(14): $s_{02} = 0.83$, i.e. quasichanneled fraction is 0.17 of whole beam intencity.

2.5. Remarks on more realistic potential

The advantage of harmonic potential is that it permits the analytical solution of motion equation. For more realistic potentials, as, for example, Moliere potential shown in Fig.2, only numerical solution can be carried out. In general, these potentials distinguish from the harmonic potential in two items.

The first item concerns the terrace field at the distance $x = a$ from the plane. Here the electric field (strength) is very small, but nevertheless it exists. On the contrary, the harmonic approximation could be chosen to eliminate the electric field at $x = a$. As the result projectiles penetrating into the terrace field at the vicinity of $x_0 = a$ are deflected outward the surface and can not reach the channel. On the contrary, the harmonic potential leads to the result that such projectiles always reach the channel, see in Fig.2.

The second item concerns the electric field at plane positions, for example, at $x = 0$ where the terrace field transforms into the channel potential. The realistic transformation both terrace-channel and channel-channel are smooth. Moreover, the strength of electric field is zero at plane positions. The harmonic potential has sharp peaks at these points. Hence, the electric field in the vicinity of plane position should be too weak to give the noticeable kick to the projectiles having $x_0 \approx 0$. On the contrary, the harmonic potential leads to the fact that such projectiles obtain largest deflection by terrace potential.

Nevertheless, one can conclude from Fig.2 the harmonic potential could be adjusted very accurate to match the realistic potential, so both peculiarities, near $x_0 = a$ and $x_0 = 0$, does not influence significantly results obtained in harmonic approximation. Of course, for more realistic potential the equations obtained for harmonic potential can be used only for estimations. For example, obviously projectile trajectories do not cross in the one point. Nevertheless, one can consider most trajectories transit through the vicinity of point $\left(x = a, z = z_{\mathrm{is}}\right)$, particles deflected

outward the surface before they can reach the channel have the maximal deflection angle about θ_{pl} and so on.

Also, one should notice the motion of particles with $x_0 = 0$ is strongly influenced by multiply scattering, i.e. by close collisions with separate crystal nuclei, rather no the averaged crystal potential. Due to the multiple scattering these projectiles could obtain the significant deflection, much larger than is predicted by the averaged potential theory for particles moving in the area $x \approx 0$. In general, the multiple scattering leads to violation of transverse energy conservation low (1). Nevertheless, the multiple scattering does not influence significantly the trajectory evaluated from the averaged potential model when the particles moves at the distance from the plane approximately exceeding the atom thermal vibration amplitude.

3. SIMULATIONS

3.1. General principles

The particle motion in the miscut surface layer, i.e. in the crystal volume where the plane lengths determined by the miscut angle successfully decrease, was investigated by numerical simulations. Herein, the crystal thickness l corresponds to the maximal plane length (see in Fig.1). The number of planes N contained in the miscut layer as well as the number of channels $(N-1)$ at fixed l is defined by both miscut angle θ_m and interplanar distance a. In order to simplify the analysis we should take into account the motion of only protons hitting the "miscut surface", thus, the beam width considered is $(N-1)a$. Therefore, particles flying above the top shortest plane in Fig.1 are not taken into account. Particles moving at distances $x > a$ above the top plane do not interact with the crystal field (in our approximation) and are not of interest. Further we are interested mainly in multiple terrace deflection when particle trajectory crosses several terrace fields. It will be shown this effect allows the large angle deflection, at $\theta > \theta_{\text{pl}}$. Particles, penetrating into the crystal field having $x_0 < a$ above the top plane, can interact only with the single-plane field. Based on the theory above we can speak that their deflection angle can not exceed θ_{pl}, see in Sec. 2.3.1. So, the detailed consideration of these particles will be omitted. Moreover, the contribution of these particles becomes negligible for large N (or, equivalently, for large l).

Following the channeling theory the evolution of proton transverse coordinate x is defined by the equation

$$\gamma m \frac{d^2 x}{dt^2} = -\frac{dU_{\text{cr}}}{dx}$$

The averaged planar potential was approximated by Moliere potential, see [8] and Fig.2. The projectile moves along the planes with quasiconstant velocity v_0 that defines the longitudinal coordinate of its trajectory as a function of time $z(t) = v_0 t$. The deviation of projectile trajectory from that defined by Eq.(1) due to the proton multiple scattering is taken into account by the technique previously described in [10,31]. The angular distribution of the beam at any fixed moment τ with respect to the crystal plane (as above we consider the (110) Si plane) is determined by the expressions $\tan\theta_i = v_{xi}(\tau)/v_0$ where $v_{xi}(\tau) = \left(dx/dt\right)_\tau$ is the transverse velocity of i-th proton at that moment. This is also valid for the moment, at which the projectile leaves the crystal through either back side or lateral miscut surface. Obviously, as above described, the first corresponds mainly to the channeled protons, while the second - to both quasichanneled in a bulk and deflected by the terrace potential protons.

In our simulations we have used non-divergent 400 GeV and 120 GeV proton beams interacting with aligned Si (110) crystal that are typical objects of recent CERN crystal

collimation experiments based on the technique of beam channeling in a bent crystal [5,6,32]. The initial beam direction was chosen to be coincided with the Z-axis, see in Fig.1, hence, the crystal field, which is mostly perpendicular to the (110) planes, has became the function of transverse coordinate x. The motion in Y-direction, which is directed along the (110) planes and transverse to the initial beam direction, is out of interest in this study and herein has not been considered. Having chosen the initial beam direction along (110) planes of aligned Si crystal, the deflection angle after proton passage through the crystal has been defined as the angle of a proton velocity with respect to the (110) plane.

3.2. Proton trajectories

Several trajectories evaluated as described in Sec. 3.1 are shown in Fig.6 together with corresponding deflection angles θ. The results are presented for 120 GeV protons, crystal has the miscut angle $\theta_m = 20$ μrad and the thickness is $l = 50$ μm. The miscut layer consists of $N = 6$ planes. The deflecting effect of miscut surface is evident. One can see trajectories B, C, D can cross several terrace fields due to quasichanneling effect. Moreover, the maximal deflection angles is given by trajectories C and D which essentially influenced by terrace fields rather no the channel field and this deflection angle $\theta \approx 35$ μrad is substantially exceeding the value 23 μrad obtained for the case when beam is deflected by the single terrace (see Sec. 2.4.2).

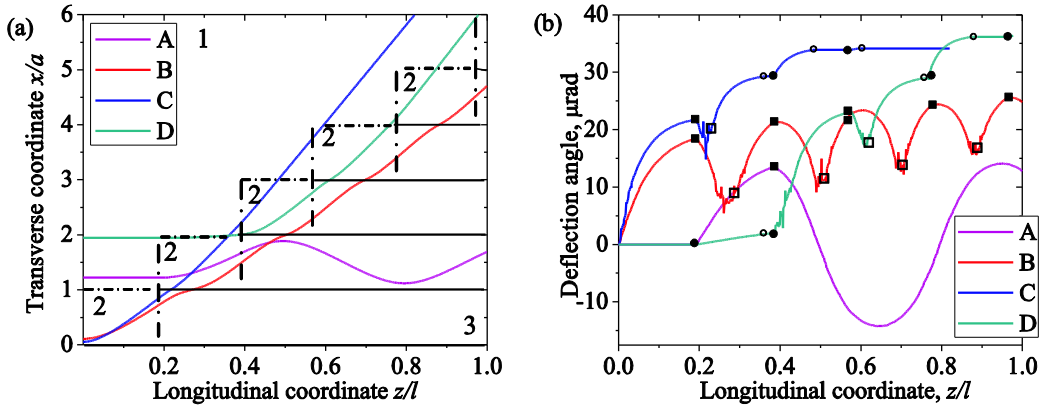

Fig. 6. (a) Samples of proton trajectories: the trajectory of channeled proton (A), the trajectories of quasichanneled protons when the proton leaves the crystal through the back side (B) or through the lateral surface (C, D). Planes are designated by horizontal black solid lines; the maximal length plane coincides with the bottom axis. Areas of different fields are delimited by dash-dot lines and are designated by numbers: 1 – field is absent, 2 – the terrace field, 3 – the channel field. (b) The deflection angles along trajectories shown in the panel (a). Symbols correspond to moments when the projectile crosses a field border: ● - proton moves from the vacuum to the terrace field, ○ - proton leaves the terrace field and exits to the vacuum, ■ - proton reaches the channel field from the terrace field, □ - proton moving in the channel field crosses the plane and falls into the terrace field. The sharp oscillations appear due to strong multiple scattering when particle is near to a plane.

One should mention here the difference between trajectories C and D. The initial point of trajectory C corresponds to strong terrace field. So, the proton gets the significant transverse velocity at the first terrace to be further quasichanneled in correspondence with the theory developed in Sec. 2.3.3. The quasichanneled proton crosses the channel border at the initial Δz section of the channel which is formed by next upper terrace of the miscut layer having the deflection angle θ. Futher the proton moves in deflecting single-plane field getting additional deflection angle $\delta\theta$. After that proton reaches next terrace (or, probably, next channel) having

grown incident angle $\theta + \delta\theta > \theta$, and so on, in correspondence with the arrow 3 in Fig.1. Hence, proton suffers multi plane deflection at large angle.

On the contrary, the proton moving along the trajectory D penetrates into the terrace field in the area of weak field at large distance from the plane. Nevertheless, this weak field of the first terrace is capable to direct the proton to the second terrace field instead of to the channel (similar to the motion of the kind 1 in Fig.1). The proton falls to the strong field of the second terrace near the plane and finally can be deflected at large angle by the way described in the previous paragraph. This kind of deflection is not predicted by harmonic potential theory described in Sec. 2.3.3 (the particles having large initial distance from the plane should be channeled), but is discussed in Sec. 2.5. One can conclude the contribution into large angle deflected fraction of the beam is made by protons having both large ($x_0 \approx a$) and small ($x_0 \approx 0$) initial distances from the plane forming the terrace field.

Finally, one should notice the terrace length at these conditions is $\Delta z \approx 10$ μm. At the distance of 1 μm about 10^4 Si atoms are placed in the crystal plane. Thus, the terrace potential can be described by continuous averaged potential. Also, due to the fact that the terrace length Δz ? a, the field at the distances $0 < x < a$ from the terrace plane can be considered to be orthogonal to the plane.

3.3. Angular distributions

The results of simulations for a final deflection angle in dependence on the initial transverse coordinate x_0 are presented in Fig.7(a,c) for 400 and 120 GeV protons correspondingly. The crystal thickness was $l = 100$ μm for 400 GeV and $l = 50$ μm for 120 GeV. The miscut angle was $\theta_m = 10$ μrad for 400 GeV and $\theta_m = 20$ μrad for 120 GeV. So, the miscut layer consists of $N = 6$ planes for both cases. The transverse coordinate is counted from the plane with a maximal length, i.e. from the lowest plane in Figs. 1 and 6(a). The separation of protons penetrating into the crystal field near the planes from the main beam is evident in agreement with the multiple terrace deflection consideration in Sec.3.2. Moreover, the corresponding angular distributions in panels (b, d) of Fig.7 demonstrate noticeable number of these protons.

In general, angular distributions make the dividing of the incident beam clear visible. The right peak corresponds to the deflection at large angles, $\theta > \theta_{\text{pl}}$ (the theory developed in Sec.2.3.1 predicts the angle of single terrace deflection can not exceed θ_{pl}). The right peak in angular distributions consists of the protons that are strongly deflected outward the miscut surface by the terraces' repelling field, in other words, the protons are reflected by the miscut end of the crystal. The fraction of deflected protons can exceed 10% of whole beam intensity. One can notice the deflection effectiveness growths when beam energy is increased. This conclusion is in agreement with the consideration in Sec. 2.3.2. Indeed, the number of quasichanneled protons growths at the beam energy increasing (parameter s_{02} falls down at $\alpha > \alpha_{m,\text{qch}}$ in Fig.5). Therefore, more protons can be deflected at large angles by few terraces as shown in Fig.6.

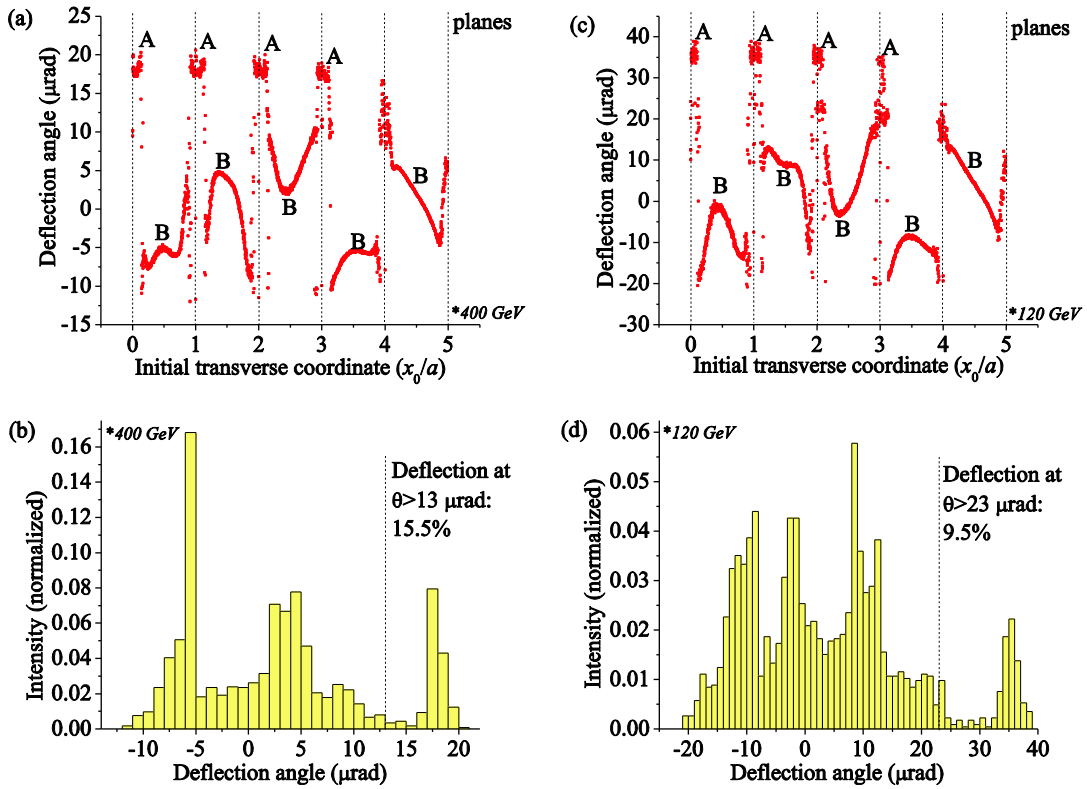

Fig.7. Scattering of initially non-divergent 400 GeV (a,b) and 120 GeV (c,d) proton beam by miscut surface. (a,c) Dependence of the deflection angle on the initial transverse particle position, i.e. on the point of penetration into the crystal: A — the deflected at $\theta > \theta_{pl}$ protons, B — the channeled protons. Positions of crystallographic planes composing the miscut surface are pointed out by vertical dashed lines. (b,d) Angular distribution of protons scattered by miscut surface: the right peak corresponds to the miscut deflected protons, while the left side of distribution - mainly to the channeled protons.

The comparison with estimations given in Sec. 4.2 shows the quasichanneled fraction is noticeably larger than the intensity of right peak in Fig.7. The discrepancy could be explained by the difference between harmonic and Molier potential. Indeed, the curve corresponded to Moliere potential harmonic is more shallow in the area B of Fig.2 that the curve for harmonic potential. Hence, the harmonic potential gives, in general, stronger electric field for the terrace field than the Moliere approximation because the strength is defined by the incline of potential curve. Hence, the particles passed the distance Δz through the terrace field obtain, as a rule, the less transverse energy (and deflection angle, correspondingly) if the crystal potential is considered in Moliere approximation in comparison with case when the harmonic potential is used.

Another cause why the large-angle-deflected fraction does not coincides with the quasichanneled fraction estimated in Sec.4.2 is the quasichanneled proton can cross the channel border at the distance larger than Δz from the channel beginning, in the point where the terrace field already does not exist. In this case proton falls into another channel and enters into the crystal bulk (as the trajectory B in Fig.6). As the result, the multiple terrace deflection becomes impossible and the proton is deflected at fewer angles.

In Fig.7(a,c) one can see, the deflection angle of group A is maximal for particles penetrating into the crystal near the bottom planes of miscut surface (as depicted in Figs.1 and 6(a)). Indeed, only protons hitting the crystal at the bottom miscut planes enable several planes crossing. Protons penetrating into the crystal at the top miscut planes do not suffer multi plane interaction due to the limited miscut layer, and are characterized by rather small-angle deflection. This is the

explanation why the deflection angle in the group A decreases when their initial transverse coordinate increases in Fig.7(a,c) tending to the value θ_{pl} at upper plane.

3.4. Dependence on miscut angle

The crystals used in channeling physics are usually characterized by a miscut angle [29]. Nevertheless, the kind of beam deflection described here has not been ever observed in channeling-related experiments. The features of beam scattering by the crystal miscut were mostly examined to prevent negative influence of the miscut to the efficiency of beam collimation based on beam halo deflection by bent crystal planes. Another point is that in performed experiments the beams enter into the crystal mainly through its front surface rather than the lateral miscut surface. Thus, the contribution of miscut deflected part becomes negligible into the total angular distribution. However, its contribution could be essential in the case of nanosize, in cross section, beams.

Fig.8 demonstrates the deflection efficiency as a function of the miscut angle. The simulations were carried out for two crystal thicknesses at 400 as well as at 120 GeV. Thicknesses $l = 100$ μm (400 GeV, Fig.8(a)) and $l = 50$ μm (120 GeV, Fig.8(b)) correspond to the simulations pointed out in Fig.7, whereas $l = 1$ mm (400 GeV) and 500 μm represent typical crystal thickness used in bent crystal collimators (see, for example, in [33] and references therein). As seen, the efficient deflection could be observed in very narrow interval of the miscut angles. The deflection efficiency falls rapidly down at the miscut angle increase, which results in decreasing the repelling field length Δz. Simultaneously, increasing the miscut angle gets growing possibility for projectiles to be trapped by the crystal bulk potentials (channel potentials); obviously, these particles will be not reflected by the miscut surface. The result is in agreement with the discussion in Sec.2.3.2 where it is demonstrated the quasichanneling disappears at large miscut angles, see in Fig.5. So, the suitable miscut angles are very small, θ_m : 10 μrad, and much less than the typical miscut angles θ_m : 100 μrad [3,29]. Additionally, the distributions in Fig. 8 exhibit there is no the deflection at large angles ($\theta > \theta_{\text{pl}}$ μrad) for very small miscut angles. It takes place due to very large terraces' lengths (see the discussion in Sec.2.3.1). Particles are deflected outward the surface by the single terrace (the type 1 of the motion) and have not the possibility to reach the planar channel. Finally, particles will be weakly reflected by the surface. The effective deflection of the beam at large angles through the particle quasichanneling (the type 3) in this case becomes impossible.

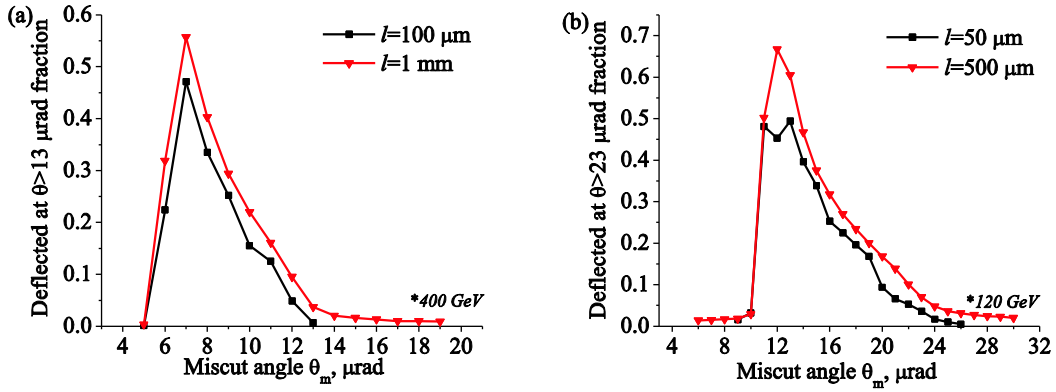

Fig.8. Fraction of protons deflected at the angles $\theta > \theta_{\text{pl}}$ μrad vs miscut angle: (a) $p_z c = 400$ GeV, (b) $p_z c = 120$ GeV.

The maximum of curves is about $\theta_{m,\text{cr}}$ (see in Sec.2.4). Indeed, at this angle $\Delta z = z_{\text{is}}$ (see in Sec. 2.3.1), i.e. following the harmonic potential theory the protons deflected by terrace field are

focused in the point where the next terrace begins (see in Fig.3). In the case of Moliere potential, when the focusing in the one point does not take place, protons, nevertheless, either leave the terrace field near the point $\Delta z = z_{is}$ or reach the channel having the transverse coordinates $x \approx a$. Both cases provide the best conditions for projectiles to enter into the next terrace field either by the way of trajectory D in Fig.6 or directly through the quasichanneling (trajectory C in Fig.6).

Strongly speaking, the fraction of large-angle-deflected protons does not tend to zero at large miscut angle. Due to multiple scattering an insignificant number of particles can always be pushed in quasichanneled regime of motion at initial channel section Δz.

Concerning the little deep in Fig.8(b) at $\theta_m = 12$ μrad and $l = 50$ μm it is the cutting effect related with the shape of distribution near deflection angle $\theta = 23$ μrad. The distributions are shown in Fig.9. At $\theta_m = 11$ μrad (a,c) the channeling is almost absent. The distribution is formed by the single peak at $\theta \approx 23$ μrad. At $\theta_m > 11$ μrad the channeling appears as well as the right peak is shifted to larger angles due to the increasing of quasichanneling role. The channeling is more important for $l = 50$ μm. In Fig.9(a,b) the border $\theta = 23$ μrad divides the right peak and only about half of the peak contributes to the fraction shown in Fig.8.(b) The channeling is absent in the panel (a) and appears in the panel (b). As the result, the fraction of projectiles deflected at $\theta > 23$ μrad is less in the case (b) in comparison with the case (a). In the panel (c) the peak is completely on the right side from the border providing the increasing of deflected at $\theta > 23$ μrad fraction in comparison with the case (b). For the case of $l = 500$ μm the channeling appearance in the panel (e) does not reduce significantly the right peak intensity in comparison with the case (d). At the same time the right shift of the peak increases the part of distribution at the right side of the border. Hence, the fraction in Fig.8(b) is larger for $\theta_m = 12$ μrad than for $\theta_m = 11$ μrad. On the contrary the shift of right peak in the panel (f) can not increase the fraction deflected at $\theta > 23$ μrad in comparison with the case (e) because the whole intensity of this peak is reduced by the growth of channeling fraction. As the result, the fraction in Fig.8(b) for $l = 500$ μm has the maximum at $\theta_m = 12$ μrad. Obviously, the maximum position in Fig.8 depends on the value of cutting angle. In particular, the little deep at $\theta_m = 12$ μrad for $l = 50$ μm in Fig.8(b) could be eliminated if one will be interested in the fraction deflected at $\theta > 24$ μrad.

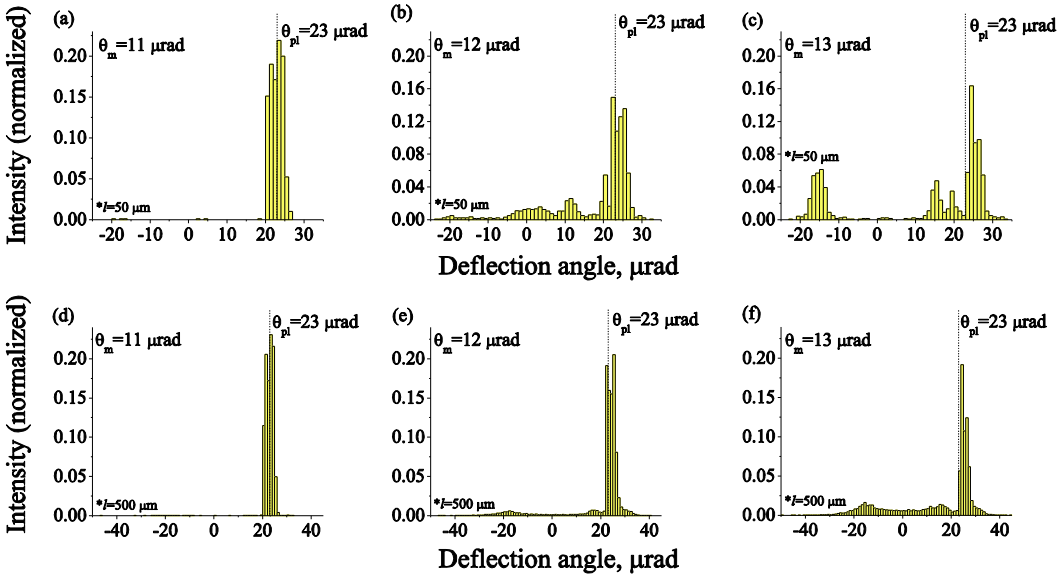

Fig.9. Angular distributions near the maximum of curves shown in Fig.8. Top panels correspond to $l = 50$ μm, bottom panels – to $l = 500$ μm.

To conclude the discussion of Fig.8, it should be underlined the range of miscut angles where the effective deflection takes place coincides almost exactly with the estimations of miscut angles interval where the quasichanneling exists (see in Sec. 2.4). It is the clear argument the deflection at large angles is provided by quasichanneling combined with the multiple terrace deflection.

3.5. Dependence on terrace number

In the Fig.8 one can see the curve corresponding to larger thickness is placed higher. The difference between that curves is the number of planes composing the miscut layer. Indeed, in correspondence with discussion above the possibility for projectile to be deflected at the large angle is minimal when the miscut layer consists of $N = 2$ planes. In the hypothetic case of infinite layer of terrace all particles following trajectories similar C or D in Fig.6(a) (or arrow 3 in Fig.1) cross the maximal number of planes and are deflected at maximal possible angle. That should result in the maximal shift of right peak in Fig.9 and, therefore, the maximal fraction in Fig.8. Nevertheless, that number of crossed planes could not be infinite and, as one can see from Fig.6, is about 3-5 at conditions considered here. So, one can assume the fraction deflected at large angles is strongly depends on the number of planes N while N is not enough to provide the maximal deflection and the fraction reaches the saturation at large N. This suggestion is approved in Fig.10. The miscut angle is considered to be fixed, the plane number N is the function of crystal length l. The slight increasing of the fraction shown in Fig.10 at large N could be explained not only by multiple terrace deflection but also by dechanneling when the channeled projectiles transits through the channeling regime of motion in the quasichanneling state due to the multiple scattering and when this transition takes place at the initial section Δz of a channel. The comparison with Fig.8 gives the growth is not significant: the same fraction equals to 0.22 at $l = 1$ mm (400 GeV) and 0.168 at $l = 500$ μm (120 GeV).

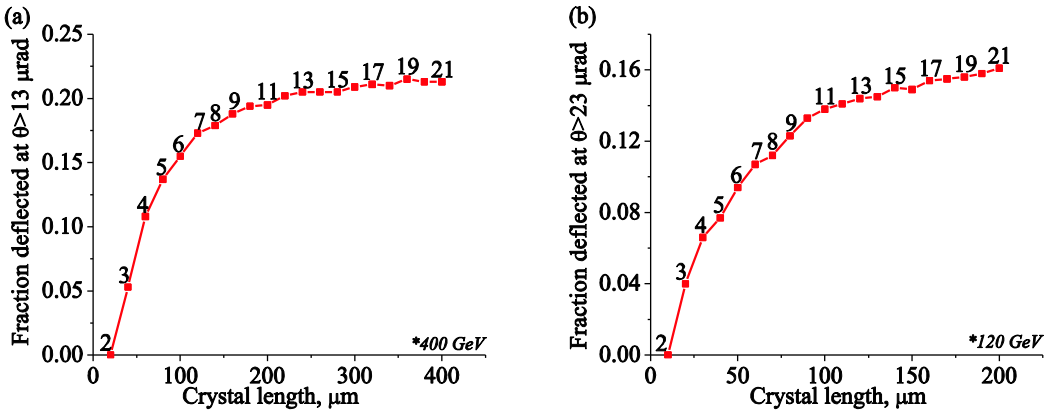

Fig.10. The fraction deflected at large angle in dependence on the crystal thickness l: (a) $p_z c = 400$ GeV, $\theta_m = 10$ μrad; (b) $p_z c = 120$ GeV, $\theta_m = 20$ μrad. The corresponding number of planes contained in the miscut layer N is pointed out near the points.

In is interesting to notice, the large-angle-deflected fraction at large N is very close to the estimations of quasichanneled fraction given in Sec.2.4.2.

4. CONCLUSION

1. The deflection of ultrarelativistic projectiles by miscut surface was approved theoretically as well as by simulations.

2. The investigations of projectiles by terrace field were carried out in details. The harmonic crystal potential was considered. The conditions of both channeling and quasichanneling were

obtained. The possibility of deflection by terrace field before the particle could reach the channel was discussed. The predictions for deflection angles were given.

3. The simulations were carried out for typical CERN energies 120 and 400 GeV. The crystal potential was approximated by Moliere potential. The multiple scattering was taken into account. The obtained results are presented in the form to be applied for experimental purpose. The results are in good agreement with theoretical predictions.

4. The effective deflection is provided mainly by quasichanneled particles. It was shown the multiple terrace reflection leads to significant increasing of the deflection angle in comparison with the single terrace deflection.

5. Usually considered that the miscut brings only negative features to the crystal fabrication. Here we have demonstrated that the miscut surface, in principle, could be used to deflect the particle beam. It is important to underline that, on the contrary to the bent crystal technology, in the case of beam deflection by the miscut surface (we can define a new technique as a ”miscut reflector”) we deal with mostly reflection of the beam from the crystal surface; there is no necessity of using the crystal bulk to control the beam. Hence, the influence of the solid on the beam (scattering, energy loss, beam intensity loss, etc.) could be essentially reduced in comparison to both beam deflection by bent crystals and beam collimation by amorphous solids [34]. The problem to observe the phenomenon is in fabricating special crystals with controlled miscut angles. Nevertheless, the progress of crystal manufacturing technologies could issue the possibility to detect described peculiarities in the nearest future.

REFERENCES

[1] E. N. Tsyganov, Fermilab preprint TM-682 (1976).
[2] C. T. Murphy et al., Nucl. Instrum. Meth. B **119**, 231 (1996).
[3] W. Scandale et al., Phys. Lett. B **714**, 231 (2012).
[4] W. Scandale et al., Phys. Lett. B **703**, 547 (2011).
[5] W. Scandale et al., Phys. Rev. Lett. **101**, 234801 (2008).
[6] W. Scandale et al., Phys. Lett. B **658**, 109 (2008).
[7] J. Lindhard, K. Dan. Vidensk. Selsk. Mat. Fys. Medd. **34**, 14 (1965).
[8] D. S. Gemmel, Rev. Mod. Phys. **46**, 129 (1974).
[9] A. M. Taratin and S. A. Vorobiev, Nucl. Instrum. Meth. B **26**, 512 (1987).
[10] A. Babaev and S. B. Dabagov, Eur. Phys. J. Plus **127**, 62 (2012).
[11] S. Baricordi et al., J. Phys. D **41**, 245501 (2008).
[12] S. Baricordi et al., Appl. Phys. Lett. **91**, 061908 (2007).
[13] E. S. Mashkova and V. A. Molchanov, Radiat. Eff. **23**, 215 (1974).
[14] A. W. Kleyn and T. C. M. Horn, Phys. Rep. **199**, 191 (1991).
[15] R. Sizmann and C. Varelas, Nucl. Instrum. Methods **132**, 633 (1976).
[16] D. Danailov et al., Nucl. Instrum. Methods B **153**, 191 (1999).
[17] D. Danailov et al., Nucl. Instrum. Methods B **164**, 191 (2000).
[18] D. Danailov, Nucl. Instrum. Methods B **264**, 29 (2007).
[19] E. B. Boyko et al., Nucl. Instrum. Methods B **256**, 359 (2007).
[20] A. Niehof and W. Heiland, Nucl. Instrum. Methods B **48**, 306 (1990).
[21] C. C. Havener et al., Nucl. Instrum. Methods B **99**, 213 (1995).
[22] F. W. Meyer et al., Nucl. Instrum. Methods B **100**, 366 (1995).
[23] A. Robin et al., Nucl. Instrum. Methods B **193**, 568 (2002).
[24] W. Heiland and A. Robin, Nucl. Instrum. Methods B **203**, 76 (2003).
[25] A. Robin and W. Heiland, Nucl. Instrum. Methods B **230**, 165 (2005).
[26] M. Hasegawa et al., Nucl. Instrum. Methods B **33**, 334 (1988).
[27] S. Baricordi et al., Appl. Phys. Lett. **87**, 094102 (2005).
[28] W. Scandale et al., Rev. Sci. Instrum. **79**, 023303 (2008).
[29] K. Elsener et al., Nucl. Instrum. Methods B **119**, 215 (1996).

[30] L. D. Doucette et al., Rev. Sci. Instrum. **76**, 036106 (2005).
[31] A. A. Babaev, Comput. Phys. Commun. **185**, 368 (2014).
[32] W. Scandale et al., Nucl. Instr. Meth. B **268**, 2655 (2010).
[33] W. Scandale et al., Phys. Lett. B **726**, 182 (2013).
[34] W. Scandale et al., Phys. Lett. B **692**, 78 (2010).